

# 10 Muon trigger chambers

## 10.1 Introduction

The detectors that provide signals to the level-1 muon trigger electronics must provide fast information on muon tracks traversing the detector in an environment of very high background. The trigger detectors must provide information that allows:

- discrimination on muon transverse momentum,  $p_T$
- bunch-crossing identification
- fast, coarse tracking for input to higher-level triggers
- second coordinate measurement in the non-bending projection with a resolution  $\sim 10$ mm

These demands define the requirements on both the time resolution (less than the bunch-crossing interval) and the spatial resolution of the detectors. Stand-alone trigger detectors are necessary since the precision muon chambers have maximum drift times much longer than the LHC bunch-crossing period of 25ns and are therefore unsuitable for bunch-crossing identification. The trigger detectors must provide acceptance in pseudo-rapidity out to  $|\eta| \approx 2.4$ , and over the full  $\phi$  range. The soft background in the cavern will induce random hit rates in the trigger detectors in the range 20–60Hz/cm<sup>2</sup> at high luminosity. This requires using a coincidence of two or more planes for at least one of the coordinates of a triggering track.

The technologies used for the trigger detectors must satisfy the above criteria and yet be suitable for mass-production in order to cover the large areas required. The solutions chosen optimize the cost of the total system, matching the rate capability and the spatial resolution to the above requirements. Since the operating conditions in barrel ( $|\eta| < 1.05$ ) and end-cap ( $1.05 < |\eta| < 2.4$ ) regions are different, different technologies are chosen for these two regions.

In the barrel, the Resistive Plate Chambers (RPCs) provide the needed time and space resolution. RPCs do not have wires and are therefore easy to construct. This allows covering large areas simply and inexpensively. They have an adequate rate capability and a very good time resolution,  $\sigma = 1.5$ ns, that allows bunch-crossing identification.

In the end-cap region, where the trigger chambers are located outside the toroidal field with a smaller separation between trigger stations, a higher granularity is needed. This need is enhanced by the higher particle momenta for the same  $p_T$  and the lower  $|Bd|$  in certain  $\eta$ - $\phi$  regions. Thin Gap Chambers (TGCs) provide this capability. Higher granularity is easily attained by the use of wires for read-out. Despite the need for high granularity, the number of electronic channels can be kept reasonably low by shifting the read-out channels by a half or a third of a channel width between layers. This ‘staggering’ of wire-groups is possible because TGCs have small group-to-group cross-talk. A smaller effective granularity is therefore achieved with a reasonable number of channels. Thin Gap Chambers also have the good time resolution required for bunch-crossing identification and a high rate capability to cope with the expected higher backgrounds in the forward region. TGCs are extremely robust and have been proven in a previous long-running experiment [10-1].



Each RPC station consists of two gas gaps with two planes of read-out strips each: one in the transverse and one in the longitudinal direction. Both planes are used in the trigger: the so called ‘ $\eta$  strips’ are parallel to the MDT wires and provide the bending view of the trigger detector; the ‘ $\phi$  strips’ are orthogonal to the MDT wires and provide the second-coordinate measurement. The  $\phi$ -strips are also needed for the pattern recognition. The RPCs are organized in several modules and their dimensions having been chosen to match those of the corresponding MDTs. In most of the stations, RPCs are composed of two units along both the azimuthal and the beam direction. To avoid dead areas between adjacent units, the active zones of neighbouring RPCs are partially overlapped in  $\eta$  as shown schematically in Figure 10-2. There is a total of 1052 chambers with close to 430,000 read-out channels. Table 10-1 summarizes the RPC strip dimensions and Figure 10-3 details the placement of the front-end boards.

**Table 10-1** RPC dimensions

number of chambers	1052
number of channels	430,000
$\eta$ strip pitch	26.2–30.0 mm
$\phi$ strip pitch	23.1–26.8 mm
$\eta$ strip length	480–1200 mm
$\phi$ strip length	970–2425 mm

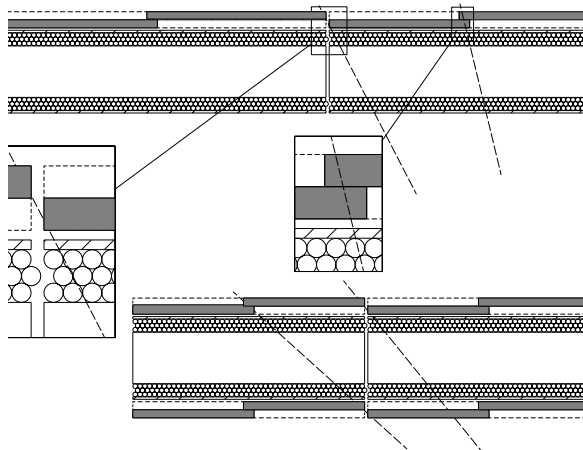


**Figure 10-2** Schematic view of the border in the  $\eta$  direction between two neighbouring chambers for the middle and outer stations.

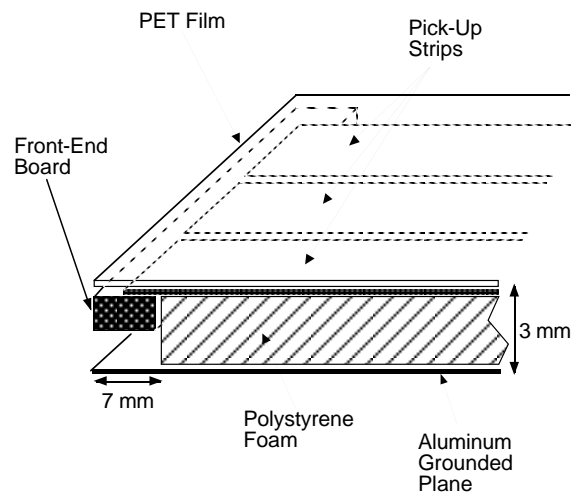


**Figure 10-3** Detail of RPC strip and front-end board placement.

### 10.2.2 End-cap

As shown in Figure 10-4, TGC trigger chambers are arranged in the ATLAS detector in seven layers in each end-cap at  $|z| \sim 14$  m. They are grouped in three planes in  $z$ : one plane of triplet units and two of doublet units. The doublet forming the plane farthest from the interaction point in each end-cap is referred to as the ‘pivot plane’, and the chamber layout and electronics are arranged such that there are no overlaps or holes in this plane. The second doublet plane and the triplet plane are separated from the pivot plane by 50 cm and 160 cm in  $z$  respectively. Neighbouring units within a plane are staggered in  $z$  to produce overlaps that prevent inactive regions creating acceptance gaps. For triggering, the TGCs cover a pseudorapidity range  $1.05 < |\eta| < 2.4$ . Each trigger plane of TGCs consists of a ‘wheel’ of eight octants of chambers symmetric in  $\phi$ . As shown Figure 10-5, each octant contains three sets of units (doublets or

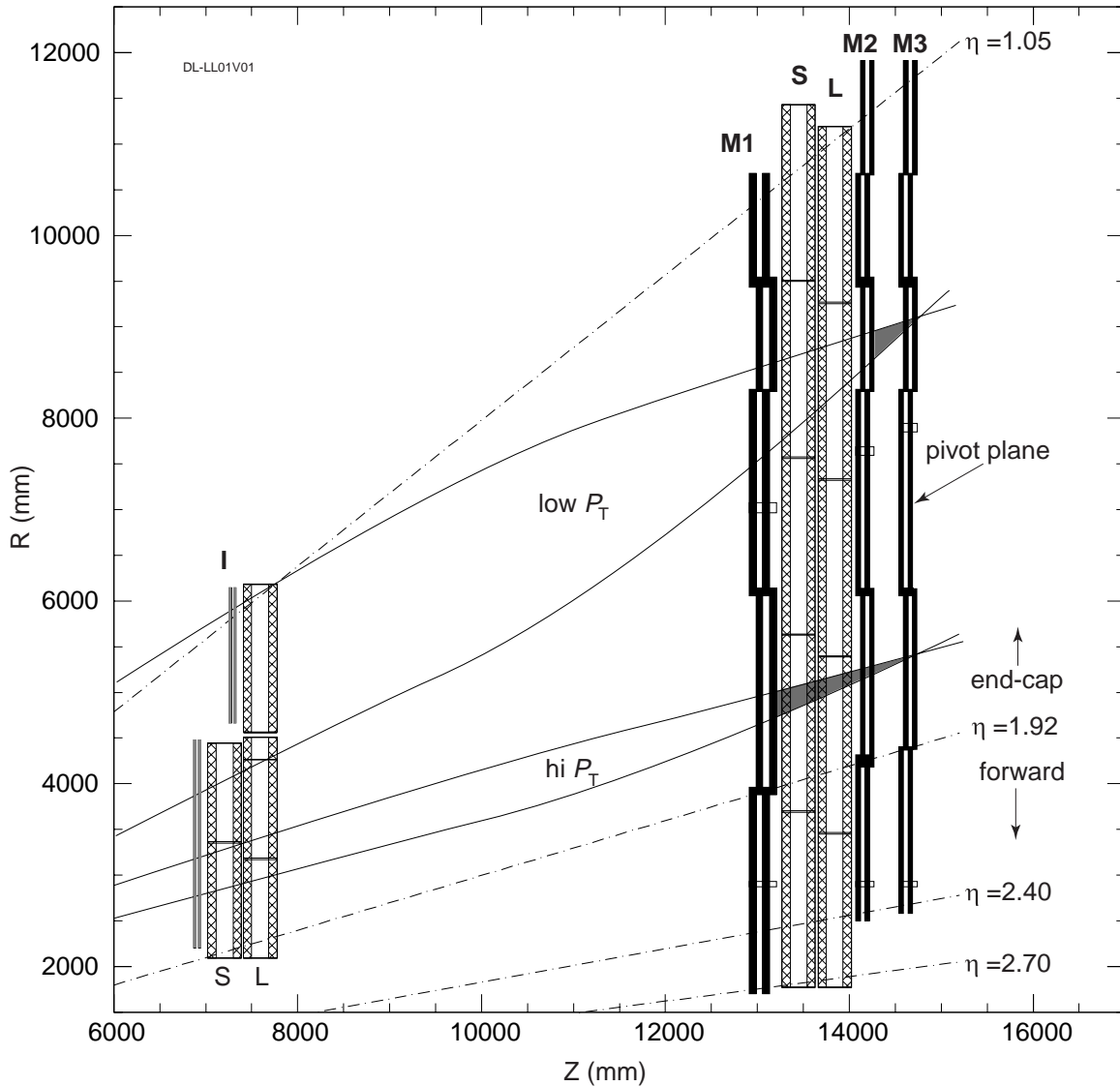


**Figure 10-4** Longitudinal view of the TGC system, showing trajectories of high and low  $p_T$  muons and their trigger windows. M1 is the TGC triplet, M2, M3 are the TGC doublets, S and L are the small and large MDTs, I is the inner-station TGC (not used in the trigger). To allow overlapping of the physical chambers, doublets and triplets at adjacent  $\phi$  are at slightly different  $z$ ; chambers at two adjacent  $\phi$ 's are shown.

triplets), where a set consists of one unit in the Forward region at high  $\eta$ , and eight or 10 units in the End-cap region. Coincidences between hits in the pivot plane and the adjacent doublet plane are used to make a low- $p_T$  threshold trigger, and those between hits in all three planes and to make a high- $p_T$  threshold trigger. The layout in  $\phi$  is such that the two end-caps are mirror images of each other so that the detector has CP symmetry.

The TGCs provide a measurement of the  $\phi$  coordinate in the inner layer, I, of the muon spectrometer, where soft backgrounds induce a hit rate exceeding  $200\text{Hz}/\text{cm}^2$ .

### 10.2.2.1 Layout changes since the Muon TDR

Some improvements have been made to the layout of the end-cap muon system since the Muon Technical Design Report [10-2]. Since each TGC station is now mounted on a single, large circular wheel, there is no longer any shift in  $z$  between the Forward and End-cap TGC sections. The consequent reduction in the number of chambers and their increased size has reduced the total area of their overlap regions. A further benefit is the reduction in the number of channels without loss of resolution. The  $\phi$  segmentation is now rationalized such that a span in  $\phi$  of two End-cap chambers is now matched by one Forward chamber, as shown in Figure 10-5.

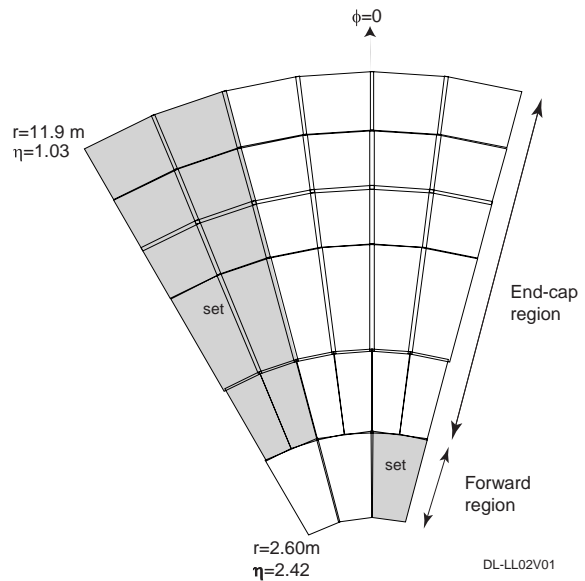


**Figure 10-5** A TGC doublet octant showing its component doublet units. The shaded areas denote a Forward set and an End-cap set. The 'double lines' are the chamber overlaps.

### 10.2.3 Combined system

The geometry of the two independent systems that constitute the muon trigger detectors has been designed to produce a global layout where acceptance is optimized without compromising the system performance. The demands for acceptance require that the two systems, barrel and end-cap, overlap in both  $\eta$  and  $\phi$  in the transition region. Care has been taken to ensure that the two sub-systems can be combined in a way that ensures good trigger performance in the transition regions, while avoiding double counting of muons. Figure 10-6 shows how the overlap is treated in  $\phi$ , where the segmentation of the TGC counters is shown for the sub-sectors of the end-cap detector. The boundaries between the RPC sectors of the barrel have been designed to map onto the boundaries between sub-sectors of the TGC. For more details, see Ref. [10-3]. The overlap in  $\eta$  can be seen in Figure 9-1 in Chapter 9.

Triggers from both sub-systems are treated similarly in the Muon to Central Trigger Processor Interface (MUCTPI) described in Chapter 13 from where they are passed to the Central Trigger Processor. In both  $\eta$  and  $\phi$ , trigger logic exists in the MUCTPI to handle triggers occurring in the overlap region to avoid double triggers from single muons.

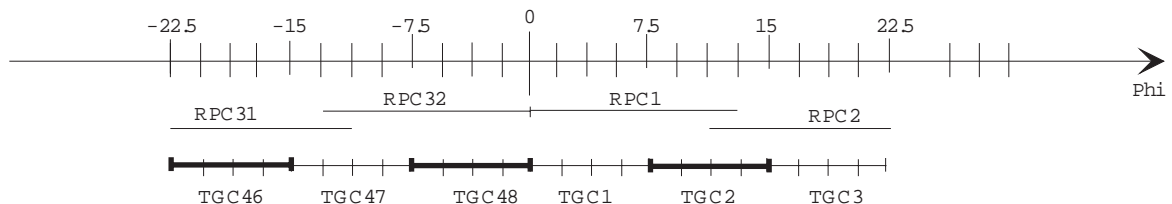


**Figure 10-6** The overlapping of the four RPC sectors in the barrel with the TGC sub-sectors of the end-cap for an octant. The TGC 'tick' marks indicate the TGC sub-sector boundaries. The boundaries between the barrel sectors have been designed to map onto the boundaries between the end-cap sub-sectors.

## 10.3 Detector characteristics

The use of two different chamber technologies in the barrel and end-cap is suited to the different granularity, rate capabilities, production capabilities and cost optimization. It also requires different matching electronics which are described in Section 10.4.

### 10.3.1 Barrel

The RPC is a gaseous detector providing a typical space-time resolution of  $1\text{ cm} \times 1\text{ ns}$  with digital read-out. The basic RPC unit is a narrow gas gap formed by two parallel resistive Bakelite plates, separated by insulating spacers. The primary ionization electrons are multiplied into avalanches by a high, uniform electric field of typically  $4.5\text{ kV/mm}$ . Amplification in avalanche mode produces pulses of typically  $0.5\text{ pC}$ . The candidate gas mixture is based on tetra-fluoroethane ( $\text{C}_2\text{H}_2\text{F}_4$ ), a nonflammable and environmentally safe gas. The signal is read out via capacitive coupling by metal strips on both sides of the detector. A trigger chamber is made from two rectangular detector layers, each one read out by two orthogonal series of pick-up strips as described in Section 10.4.1. RPCs have a simple mechanical structure, use no wires, and are therefore simple to manufacture. The  $2\text{ mm}$  thick Bakelite plates are separated by polycarbonate spacers of  $2\text{ mm}$  thickness which define the size of the gas gap. The spacers are glued on both plates at  $10\text{ cm}$  intervals. A  $9\text{ mm}$  wide frame of the same material and thickness as the spacers is used to seal the gas gap at all four edges. The RPC performance specifications are summarized in Table 10-2.

**Table 10-2** RPC performance specifications

Intrinsic detector efficiency (single layer)	98.5%
Efficiency including spacers and frames	>97%
Intrinsic time jitter (within $3\sigma$ )	<5 ns
Time jitter including strip propagation	<10 ns
Rate capability	$\sim 1\text{ kHz/cm}^2$
1 MeV photon sensitivity	1%
Gas gap	2 mm
Operating voltage	$\sim 9.0\text{--}10\text{ KV}$

The outside surfaces of the resistive plates are coated with thin layers of graphite paint which are connected to the high-voltage supply. These graphite electrodes are separated from the pick-up strips by  $200\ \mu\text{m}$  thick insulating films which are glued on both graphite layers. The read-out strips are arranged with a pitch varying from  $23.0\text{ mm}$  to  $30.0\text{ mm}$ .

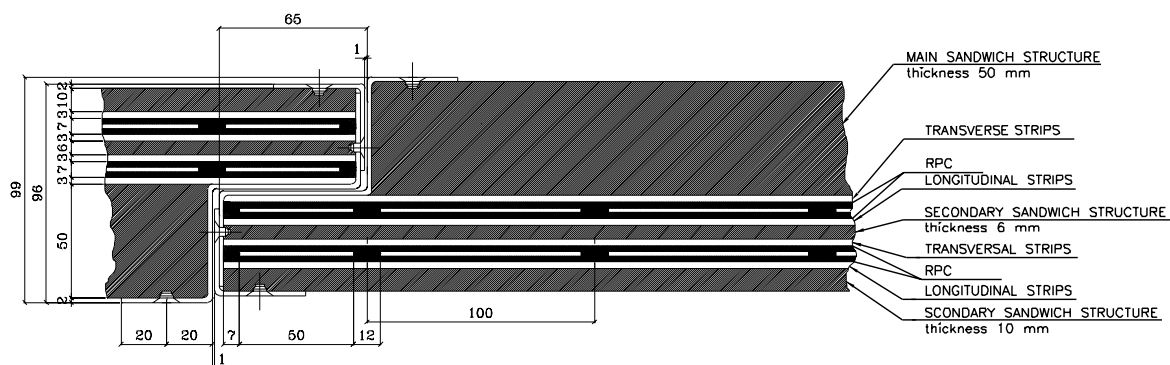


**Figure 10-7** Schematic representation of a trigger station in the barrel system.

Each trigger station is made from two detector layers and four read-out strip panels. These elements are held together rigidly by two support panels which provide the required mechanical stiffness of the chambers. The panels are made of polystyrene sandwiched between two aluminium sheets. The mechanical structure of an RPC chamber is shown in Figure 10-7; the total thickness is 100 mm.

The RPCs will be operated with a gas mixture of tetra-fluoro-ethane,  $C_2H_2F_4$ , and a small component of isobutane,  $C_4H_{10}$ , (97:3), with a total gas volume of 18 m<sup>3</sup>. Recent laboratory tests have shown that the addition of a small amount of sulphur hexafluoride ( $SF_6$ ) makes the mixture streamer-less for a large voltage range [10-4]. In Figure 10-8 the RPC efficiency and streamer probability are plotted as a function of the applied voltage for the  $C_2H_2F_4/C_4H_{10}$  mixture, with and without  $SF_6$ . The gas mixture with e.g. 1% of  $SF_6$  gives about 1kV high-voltage plateau in pure avalanche operation.

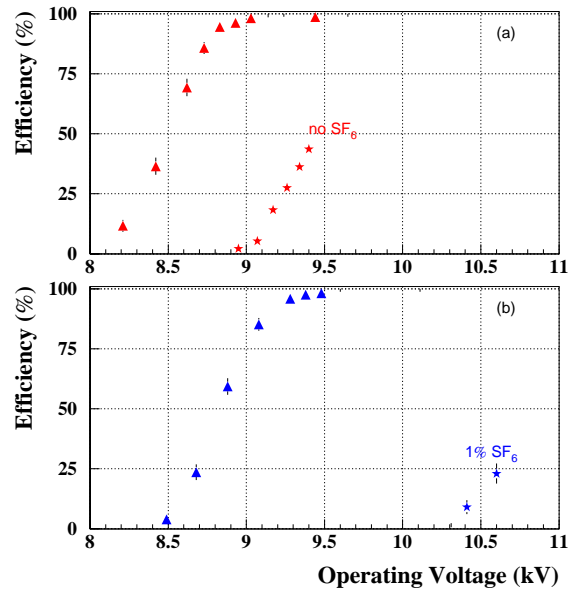


**Figure 10-8** RPC efficiency and streamer probability as a function of operating voltage, without (a), and with (b), the addition of 1%  $SF_6$  to the standard gas mixture.

### 10.3.2 End-cap

Thin Gap Chambers are similar to multi-wire proportional chambers but with an anode wire pitch greater than the anode-cathode distance. The gas used in the chambers is a highly quenching mixture of  $CO_2$  (55%) and *n*-pentane (45%) permitting operation in a saturated mode. This combination of gas and geometry offers small sensitivity to deformation, small dependence of pulse height on incidence angle and a Gaussian pulse-height distribution with no streamer formation. Signals from anode wires and from read-out strips orthogonal to these wires provide bunch-crossing identification with an efficiency greater than 99% for the 25 ns gate of ATLAS [10-5]. The use of wires enables high granularity with very small cross-talk between wire-groups (<3%). The use of a strongly quenching gas combined with the fast response of the TGCs allow operating at rates exceeding 20kHz/cm<sup>2</sup>.

**Table 10-3** Principal TGC parameters.

Gas gap	2.8mm
Anode wire pitch	1.8mm
Wire diameter	50µm
Wire potential	3100V
Gas mixture	$CO_2/n-C_5H_{12}$ (55%/45%)
Gas amplification	$10^6$
Anode r/o pitch	7.2 – 39.0mm
Time resolution	> 99% efficiency for 25ns gate
Rate capability	tested at 30kHz/cm <sup>2</sup>
Read-out strip width	14.6–49.1mm
Total number of anode r/o channels	280 000
Total number of strip r/o channels	95 000

The chambers are constructed from a plane of anode wires sandwiched between cathode planes of graphite coated glass-epoxy laminate (FR-4). TGCs are built as units of doublets or triplets, with the two or three gas gaps within a unit separated by 20mm thick paper honeycomb. Several anode wires are fed to a common amplifier-shaper-discriminator for input to the trigger electronics. The number of wires per group varies according to the desired granularity as a function of pseudorapidity. The structure of the chambers is shown in Figure 10-9 and the parameters of the chambers are summarized in Table 10-3.

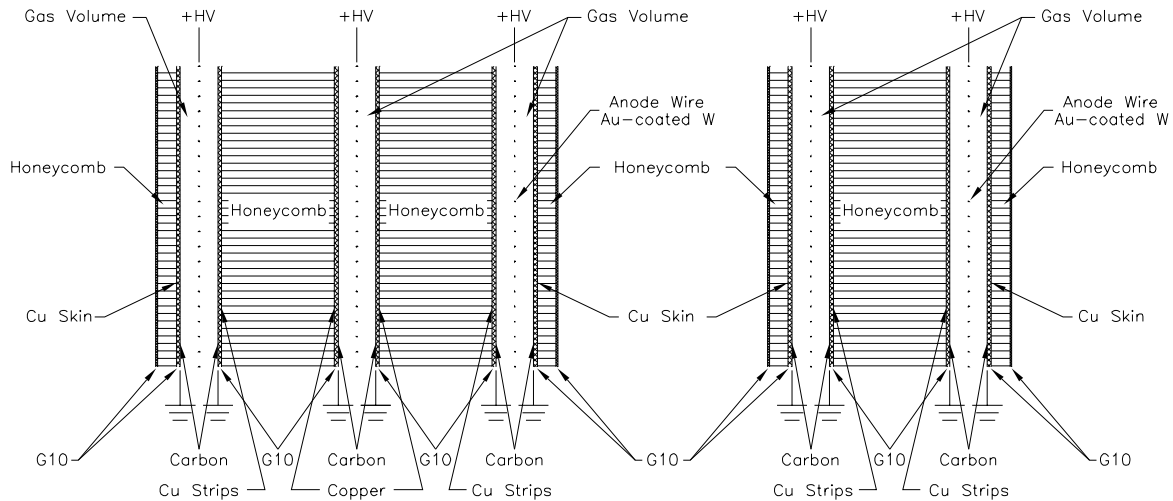


**Figure 10-9** Cross-section of a triplet (left) and of a doublet (right) of TGCs. Note that the triplet has strips for the azimuthal coordinate read-out on the two outer layers only. (The gas gap is not drawn on the same scale as the other elements.)

## 10.4 Front-end electronics

### 10.4.1 Barrel

A RPC operating in avalanche mode produces typically a single signal of 5ns FWHM and 1.5ns time jitter. A typical RPC timing distribution for the measured time-difference between two detectors for normally-incident particles in a beam-test is shown in Figure 10-10.

**Table 10-4** RPC front-end electronics and signal specifications.

Input voltage threshold	150 mV
Shaping time	5 ns
Time skew	<100 ps
Dissipated power	<50 mW/ch

To preserve the excellent intrinsic time resolution of the RPCs, the read-out strips are optimized for good transmission properties and are terminated at both ends to avoid signal reflections. The strips have a pitch between 2.3cm and 3.0cm. The front-end electronics is based on an eight channel chip which is mounted on boards fixed at the edge of the read-out panel between the strip and the ground planes. The boards are 3mm thick to fit the read-out panel thickness and 1cm wide. The length of the boards is tuned with the width of the strips so that each board input is essentially in contact with the corresponding strip and no connection wires are required. The input-to-output delay is the same for all eight channels. The front-end circuit is a three-stage voltage amplifier connected to a variable-threshold comparator. Figure 10-11 shows the block scheme of the front-end amplifier. It is implemented in GaAs technology. The amplifier frequency response was optimized for the typical time structure of the RPC avalanche signal according to the following conditions:

- same rise-time for the amplified and the input signals
- minimum return-to-zero time for the output signal

The resulting frequency response has a maximum at 100MHz and a 3dB bandwidth of 160MHz. The amplifier output is bipolar giving zero integrated charge thus avoiding a possible dependence of the steady output voltage on the counting rate. A two-channel, full-custom prototype chip of the front-end circuit has been manufactured in 0.7 mm GaAs technology. This chip, which is a preliminary stage before the final eight channel version, has been successfully tested on board and also mounted on the detector for cosmic-ray and beam tests [10-6]. Electronic and signal specifications are summarized in Table 10-4.

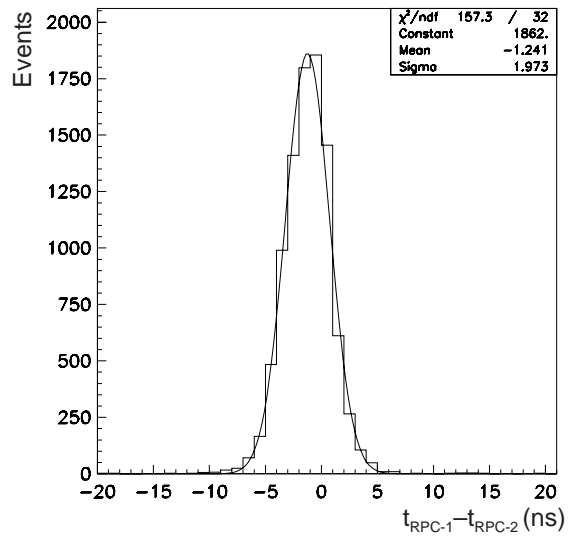


**Figure 10-10** Time-of-flight between two RPCs. The resolution of one chamber is the  $\sigma$  of the Gaussian fit divided by  $\sqrt{2}$ .

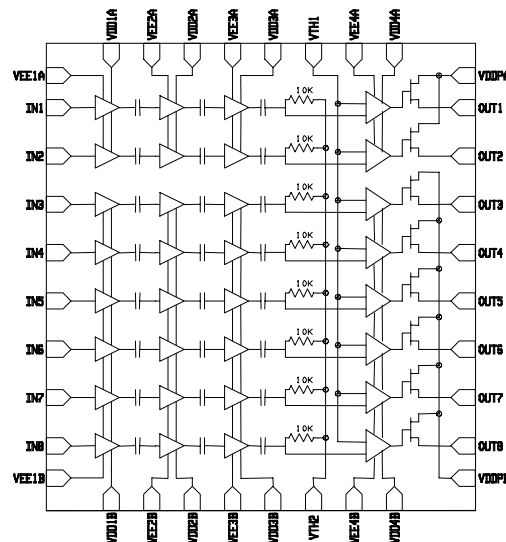


**Figure 10-11** Block diagram of the 8-channel chip front-end amplifier for the RPC system.

### 10.4.2 End-cap

Signals for the level-1 muon trigger system in the end-cap come from TGC chamber anode wires and from strips. Several wires (the number depending on the granularity required as a function of  $\eta$ ) are ganged together to provide an anode signal. Wires are spaced 1.8mm apart and the cathode plane is 1.4mm from the anode wires. Detector and signal parameters of TGCs are shown in Table 10-5.

**Table 10-5** Detector and signal parameters of TGCs.

Anode wire length	39–167 cm
Number of wires per group	6–20
Strip length	104–216 cm
Wire-group capacitance	22–390 pF
Strip capacitance	50–60 pF
Wire propagation velocity	27 cm / ns
Total wire signal (electrons in 5 ionization clusters)	$1 \times 10^7$
Total strip signal (electrons in 5 ionization clusters)	$2 - 5 \times 10^6$

The timing resolution of the system is such that there is a 99% efficiency for signals arriving within the 25 ns gate (for perpendicular tracks). The measured arrival time distribution is shown in Figure 10-12. The tails of the timing distribution are mostly due to particles traversing the chamber in the low electric field regions midway between wires, a phenomenon that will be minimized in ATLAS due to the angle of incidence of muons into the TGC counters ( $>10^\circ$ ). The ASD circuit has a negligible effect on the timing resolution.

The signals emerging from the chambers are fed into a two-stage amplifier in an amplifier-shaper-discriminator (ASD) circuit [10-7]. Four such circuits are built into a single ASD chip and four ASD chips incorporated into an ASD board. Each such 16 channel ASD board is attached to the edge of a TGC. The final prototype of the ASD chips has been produced and incorporated into the prototype of the ASD board. A number of such ASD boards were tested together with a full-size prototype TGC doublet and triplet and operated successfully at a threshold of  $3\sigma$  above the thermal noise. There will be a total of  $\sim 24500$  ASD boards corresponding to  $\sim 375,000$  signals input to the trigger logic from the TGC wires and strips.

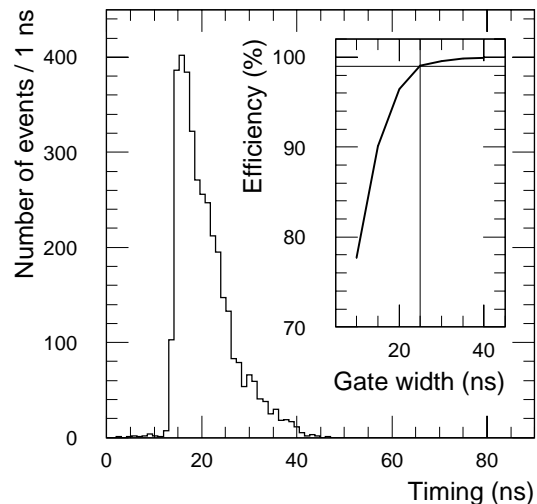


**Figure 10-12** Measured arrival time distribution for a minimum-ionizing particle, and the fraction of the arrival times that are within the given time width. There is 99% efficiency for a gate width of 25 ns, at  $0^\circ$  incident angle.

## 10.5 References

- 10-1 G. Mikenberg et al., *Thin-gap gas chambers for hadronic calorimetry*, Nucl. Instrum. Methods A265 (1988) 223.
- 10-2 *ATLAS Muon Technical Design Report*, CERN/LHCC/97-22, May 1997.
- 10-3 P. Farthouat, *Current Understanding of the Muon Level-1 System*, Revision 2, ATLAS note DAQ-NO-089, May 1998.
- 10-4 P. Camarri et al., *Streamer suppression with SF<sub>6</sub> in RPCs operated in avalanche mode*, (to be published in Nucl. Instrum. Methods).
- 10-5 Y. Arai et al., *Timing optimization of thin gap chambers for the use in the ATLAS muon end-cap trigger*, Nucl. Instrum. Methods A367 (1995) 398-401.
- 10-6 R. Cardarelli et al., *RPC front-end electronics for the ATLAS Level-1 Trigger Detector*, Proc. of the 7th Pisa Meeting on Advanced Detectors, Isola d'Elba, May 1997, to be published in Nucl. Instrum. Methods.
- 10-7 O. Sasaki et al., *Front-end electronics for the Thin Gap Chambers (TGC) in ATLAS forward muon trigger system*, CERN / LHCC / 96-39, Second Workshop on Electronics for LHC Experiments, Balatonfüred, Hungary, September 1997.

